Catalysis Letters Vol. 110, Nos. 3–4, September 2006 (© 2006)
DOI: 10.1007/s10562-006-0117-8

Spatial and temporal profiles in millisecond partial oxidation processes

Raimund Horn, Nick J. Degenstein, Kenneth A. Williams, and Lanny D. Schmidt*

Department of Chemical Engineering and Materials Science, University of Minnesota, Minneapolis, MN 55455-0132, USA

Received 18 April 2006; accepted 14 June 2006

Methods are presented to measure axial species and temperature profiles within catalytic partial oxidation foam monoliths at atmospheric pressure with 0.3 mm spatial resolution using a capillary sampling technique with a quadrupole mass spectrometer. The system allows sampling within the catalyst with negligible interference in flow or temperature by using a 0.6 mm quartz capillary containing a thermocouple and possessing a 0.3 mm side orifice. The capillary tightly fills a concentric channel drilled within the 10 mm long ceramic foam minimizing gas bypass. This technique has been used to measure axial catalyst species profiles at temperatures up to 1300 °C for catalytic partial oxidation of methane and ethane to synthesis gas and ethylene, respectively. CH_4 and O_2 conversion are approximately twice as fast on Rh than on Pt. For C_2H_6 the reaction products at the catalyst entrance are H_2, H_2O, CO, and CO_2. Ethylene production begins only after ~4 mm into the catalyst after most of the O_2 has reacted. Transient operation where the feed composition is varied stepwise between different C/O ratios has also been used to characterize these systems. The capillary sampler has a time resolution of ~0.05 s, and C/O step changes within 0.5 s have been achieved using mass flow controllers. For switches from C/O = 0.6 to 1.4, sharp overshoots are observed for syngas (H_2 and CO) and similar undershoots for combustion products (H_2O and CO_2). By placing the sampling orifice at different positions and stepping the C/O ratio, spatio-temporal profiles can be obtained. Spatio-temporal profiles are extremely important in validating detailed reaction mechanisms because their information content is much higher compared to integral steady state measurements at the reactor outlet. The spatial profiles show where and how quickly different species are formed or consumed along the catalyst axis. Transient profiles provide additional diagnostics of mechanisms and surface coverages because they show how temperature and species concentrations follow a perturbation from steady state.

KEY WORDS: catalytic partial oxidation; spatial profiles; spatio-temporal profiles; mass spectrometry; methane; ethane; syngas; ethylene; platinum; rhodium.

1. Introduction

Autothermal millisecond catalytic partial oxidation (CPO) reactors have great promise to replace steam reformers and steam crackers for production of hydrogen and olefins, respectively, because they operate at much shorter residence times, require much simpler equipment, and can be scaled up or down for different applications [1–4]. In spite of several decades of research on millisecond reactors, many questions remain concerning the mechanism of the processes. A major challenge is that the processes cannot be decomposed into simple laboratory experiments from which kinetics and catalysts can be examined systematically. This is because realistic temperature and concentration profiles cannot be created without the presence of mass and heat transfer control that change the process significantly. As examples, temperatures above ~800 °C are required to prevent total oxidation and carbon formation within the catalyst. Large gradients in temperature and concentration are necessary to prevent combustion before the catalyst and to quench primary products after the catalyst.

Detailed modeling with plug flow and two dimensional simulations has been fairly successful in simulating methane to syngas [5–9] and ethane to ethylene [10–12] over Rh and Pt catalysts using up to 100 steps for surface reactions and hundreds of steps for homogeneous reactions. While these simulations predict conversions and selectivities very accurately, typically only experimental exit compositions (integral data) were used for validating the postulated mechanisms because little information has been available regarding compositions within the catalyst.

Numerous studies have been performed to determine axial temperatures (gas and surface) within working catalysts; however, high-resolution differential composition profiles are lacking. Temperatures have been measured in extruded monoliths, fixed beds, or gauzes with IR thermography and thermocouples [13–17], but these experiments may introduce radiation and conduction losses compared to insulated catalysts. One dimensional heterogeneous simulations of a fixed bed coupling surface chemistry with intra-catalyst transport and external heat loss show that the experimentally

*To whom correspondence should be addressed.
E-mail: schmi001@umn.edu

measured gas and surface temperatures can be quantitatively reproduced [18]. Axial species profiles have been estimated by measuring exit compositions with different thickness monoliths [19] or with sphere beds of different lengths [20], but these do not necessarily duplicate the profiles within a single catalyst. Axial fuel conversion profiles were measured for natural gas on Pt coated honeycomb monoliths and simulated using detailed heterogeneous surface chemistry [21]. Species concentration profiles for methane oxidation on Rh at high pressure have been measured by gas chromatography sampling between multiple metal catalyst screen layers [22]. Plug-flow simulations with C_1 chemistry on Rh [23] were compared to the axial measured profiles [22]; however, because the experimental profile resolution was low (2 mm), both direct and indirect surface models can predict the differential experimental data since O_2 disappears within 1 mm under the conditions typically examined.

High-resolution spatial profile sampling has been used to distinguish and validate heterogeneous and homogeneous mechanisms for methane oxidation in stagnation flow and catalytic channel reactors. A stagnation flow reactor (planar catalyst) with a quartz microprobe and mass spectrometer was used to study the catalytic combustion of methane at atmospheric pressure on a hexaaluminate catalyst [24,25]. Raman and laser induced fluorescence measurements over the catalyst boundary layer in a laminar channel flow reactor have been performed from 1 to 16 bar [26,27]; these measurements were used to test the performance of surface and gas phase chemistry mechanisms at high pressure. Additionally, the axial variation of the oxidation state for a Pt/Rh catalyst [28] and the axial/radial variation of the oxidation state for a Rh catalyst [29] were measured for the methane CPO using X-ray absorption spectroscopy.

From these studies, it is clear that high-resolution spatially-resolved experimental data is key to discriminate between a number of multi-step surface mechanisms that predict integral data equally well. In this paper, high-resolution ($\sim$0.3 mm) measurements of composition and temperature profiles within autothermally operated ceramic foam catalysts are demonstrated. The capillary technique developed for this purpose perturbs the concentration, flow, and temperature fields only minimally. The method has been tested using several different geometries of sampling and several different catalysts and flow conditions. The spatial and spatio-temporal data presented allow a more stringent test for surface mechanisms describing short-contact-time reactions such as methane to syngas and ethane to ethylene.

2. Materials and methods

2.1. Monolith/catalyst preparation

Rhodium or platinum catalytic monoliths were prepared using the incipient wetness method by applying rhodium nitrate or dihydrogen hexachloroplatinate to bare α-alumina 80 or 45 pore per linear inch (ppi) monoliths. Washcoat was applied as a slurry of γ-alumina powder in water. Rh catalysts were calcined at 600 °C after washcoat application and again after catalytic metal application. The identical catalyst preparation technique has been described in more detail elsewhere [30]. For Pt catalysts, the washcoat is applied in the same way, but the Pt precursor was reduced in H_2 flow for 5 h at 500 °C to reduce Pt loss during calcination [31].

After application of catalytic materials, channels were drilled using a diamond tipped drill bit. Ideally the diameter of the drilled channel should be just barely larger than the outside diameter (OD) of the capillary so that the capillary can slide smoothly inside the monolith while minimizing gas bypass in the channel (Figure 1a and b). For the data presented here, channels were made using a 0.74 mm drill bit.

2.2. Reactor, capillary and thermocouple access

The reactor configuration and reactor materials were similar to those used in previous work described in detail elsewhere [32,33]. However, the product sampling system is a new feature (Figure 1). The sampling capillaries used were fused silica GC capillary columns having a polyimide coating on the outside that made the capillary flexible for handling but burned off quickly during the first use. An orifice was cut in the side of the capillary through which the gas sampling occurred, and the end of the capillary was sealed. The size of the orifice in the side of the fused silica tubing was $\sim$0.3 mm in diameter (Figure 1b).

The capillary exited the reactor by passing through the capillary port, a small stainless steel tube, $\sim$0.8 mm ID, which entered the lower end of the reactor through a septum. The fused silica column was connected to the top of an axial positioning system used to move the capillary/thermocouple assembly along the reactor axis. The axial positioning system consisted of a micro-volume tee fitting mounted to a linear translation stage. Data was collected by moving the translation stage stepwise in either the positive or negative direction which yielded equivalent reactor temperature and species profiles (data not shown). A thin K type thermocouple (0.254 mm OD) was inserted through the bottom port of the tee and ran up through the quartz capillary with the end of the thermocouple located at the same position as the capillary side sampling hole. The third

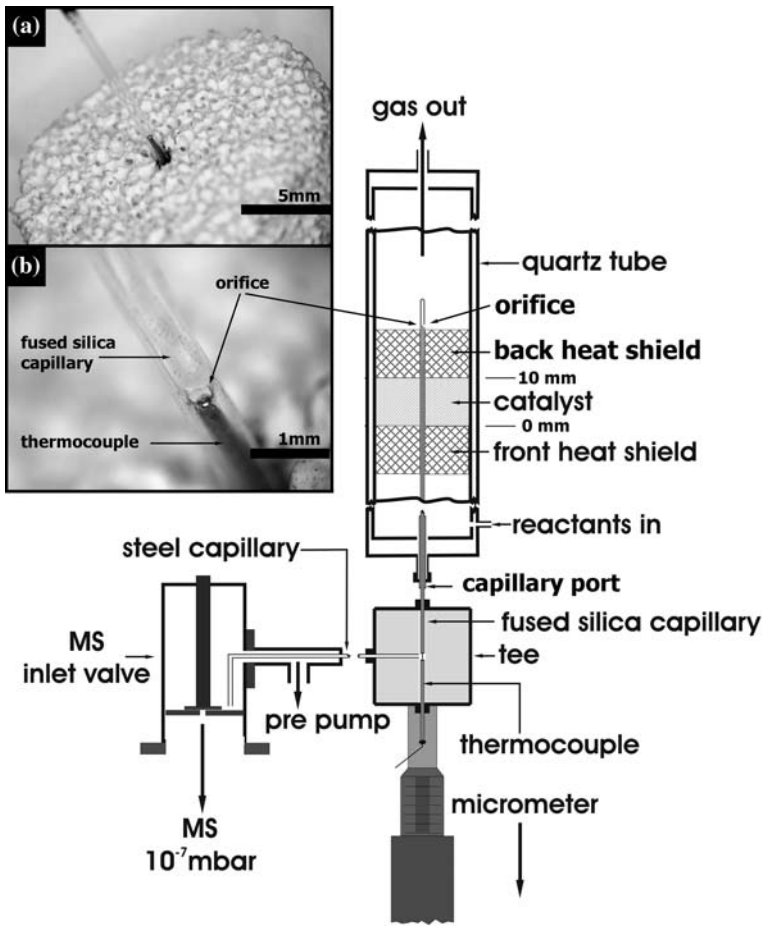

Figure 1. Schematic of the axial sampling system showing the interface with the reactor and vacuum system to collect spatially-resolved temperature and species data. Inset (a) and (b) show the channel in the monolith, the fused silica capillary, the sampling orifice, and the thermocouple.

port on the tee was connected to a stainless steel capillary (ID = 0.254 mm), which was connected to a rough vacuum pump and a leak valve leading to a high vacuum chamber containing the quadrupole mass spectrometer.

2.3. Reactor operation

Reactant gases CH_4, C_2H_6, O_2, and Ar were fed *via* calibrated mass flow controllers. Feed stoichiometry was specified as the ratio of the carbon atoms fed to oxygen atoms fed (C/O ratio). In methane experiments, argon and oxygen were fed at a ratio of 3.76:1 to simulate air. The ethane experiment was performed with ethane and oxygen at 12% argon dilution. All steady state experiments were performed at a total flow rate of 5 standard liters per minute (slpm). Before collecting any data, the reactor was run for 5–10 min to ensure the system had reached steady state.

Transient experiments were performed by changing the C/O ratio between 0.6 and 1.4 as a step function. The C/O ratio was changed by stepping the set point of the CH_4 mass flow controller but not the set point of the other mass flow controllers. Therefore, the total flow rates change slightly during the transient experiments (5.06 l/min at C/O = 0.6, 6.42 l/min at C/O = 1.4). After monitoring the steady state performance of the reactor for 20 s at C/O = 0.6, the CH_4 flow (O_2, Ar flow constant) was switched periodically between C/O = 0.6 and C/O = 1.4 giving an average C/O of 1.0. Each C/O ratio was held for 20 s. Spatially resolved transients were obtained by performing the step sequence at 15 different axial positions in the catalyst/heat shield stack.

2.4. Data analysis

The quadrupole mass spectrometer (QMS) used for data acquisition was a UTI Model 100C with electron impact ionization of 70 eV. During data collection, the pressure inside the QMS vacuum chamber was kept at $\sim 10^{-7}$ torr. The QMS unit was computer-controlled *via* Labview®. In the steady state experiment about 100 spectra were averaged to determine the molar flow rates at each location in the catalyst. In the transient experiments each data point was used independently taking advantage of the fast-sampling ability of the QMS system.

The argon signal (m/z = 40 amu) was used as an internal standard to correct for changes in the total flow rate by chemical reactions. Binary mixtures of each individual component with argon were fed into the MS to determine argon normalized sensitivity values at each m/z value of interest. This array of sensitivities was used to calculate species flow rates as is standard for quantitative analysis of hydrocarbon mixtures [34,35]. The water flow rate was determined by closing the oxygen balance. Using this calibration and analysis technique the carbon balances closed to $< |\pm 5\%|$ while the hydrogen balance closed to $< |\pm 10\%|$.

3. Results

3.1. Steady-state profiles

3.1.1. Methane CPO on Pt and Rh

Figure 2a shows the partial oxidation of methane on a Pt coated 80 ppi foam without application of a

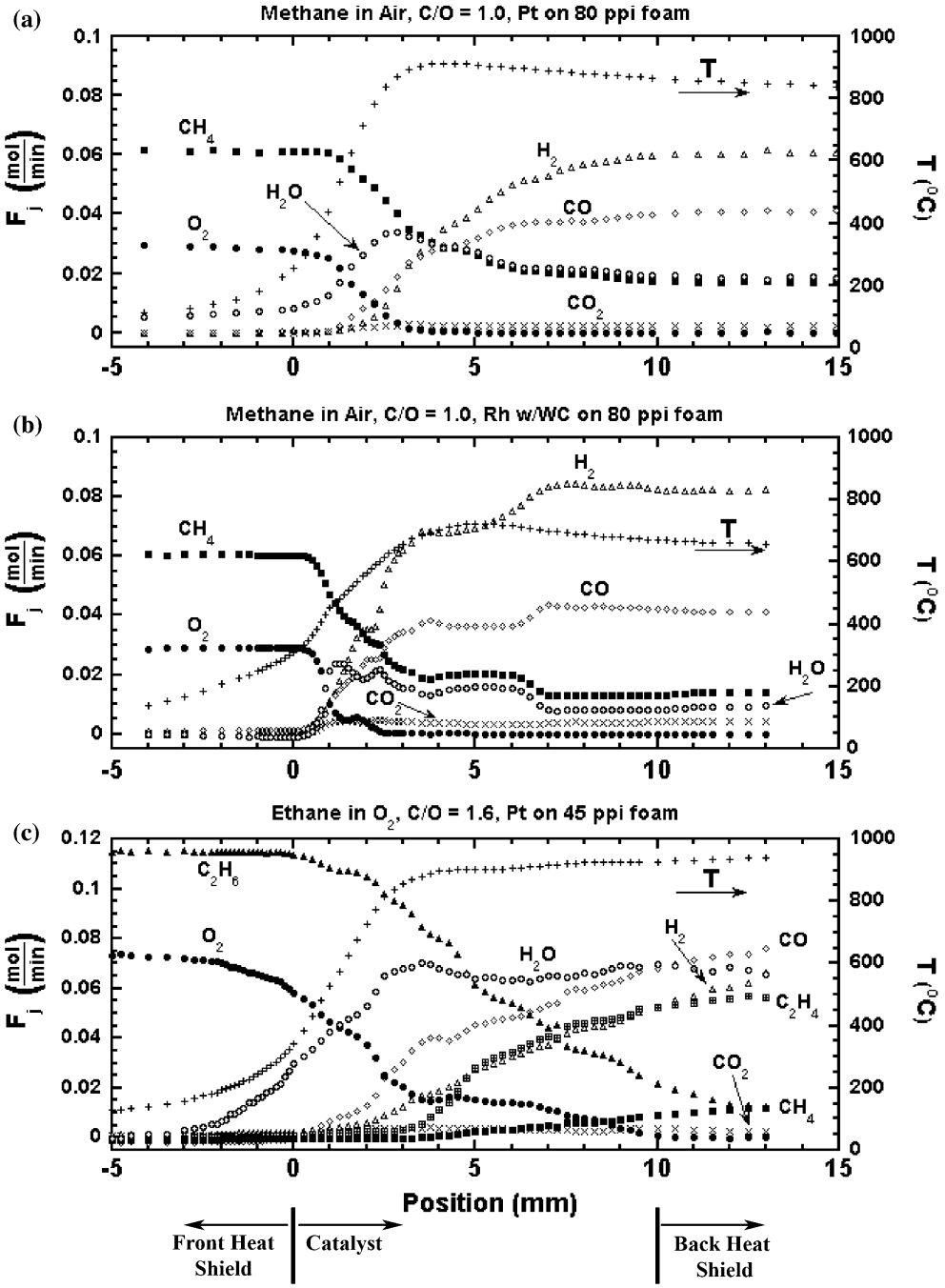

Figure 2. Species and temperature profiles for (a) methane on Pt, (b) methane on Rh with washcoat, and (c) ethane on Pt. All profiles were taken at a total 5 slpm total flowrate.

washcoat. Two distinctly different zones within the catalyst are apparent. The first zone is a 3 mm oxidation zone showing consumption of CH_4 and O_2 and production of CO, H_2, and H_2O, all in equal molar amounts. The exothermic chemistry of this zone causes the temperature to rise very quickly to ~900 °C at ~4 mm inside the catalyst. The second zone is characterized by methane steam reforming stoichiometry. A temperature decrease in this zone is observed due to the endothermic chemistry. Syngas is formed over the entire catalyst length. After the catalyst, the products do not change noticeably as expected in the absence of homogeneous chemistry.

In comparison, the profile for the partial oxidation of methane on a Rh coated 80 ppi foam with alumina washcoat (Figure 2b) shows more fine structure than the Pt profile. Most notable features are the plateau in oxygen conversion at ~1.5 mm and the methanation bump starting at ~4 mm and ending at ~7 mm, both of which are reproducible features. Although this profile appears to be more complex as compared to figure 2a, the same oxidation zone and reforming zone features are present. However, the catalyst here seems to be much more active, producing higher amounts of H_2 and lower amounts of H_2O in only 4 mm at significantly lower temperatures. Final species concentrations are reached after 7 mm.

3.1.2. Ethane on Pt

Figure 2c shows results from ethane partial oxidation on a Pt 45 ppi catalyst (no washcoat) at C/O = 1.6 with 12% argon dilution. In contrast to methane oxidation on 80 ppi foams, oxygen is converted over the entire length of the catalyst. The O_2 conversion rate is much higher from 0 to 3 mm than from 3 to 10 mm. In the first 3 mm, H_2O and CO are the main oxidation products with little H_2 production. The decrease in the O_2 conversion rate at 3 mm goes along with an onset of C_2H_4 formation with CO and H_2 being produced at approximately the same rate. A small amount of CH_4 is also produced after 3 mm. The temperature continues to rise slowly from 3 mm to the end of the catalyst and even in the back heat shield indicating global exothermic chemistry. After the catalyst, there is significant ethane conversion and ethylene formation indicating the importance of homogeneous reactions for C_2 chemistry.

3.2. Transient operation: methane on Rh

Figure 3 shows the species and temperature transients measured at the catalyst exit (x = 10 mm) for a stepped C/O ratio experiment between C/O = 0.6 and 1.4. The feed gas flow rates and the calculated C/O ratio are shown in the upper left panel. The first 20 s in this experiment represent the steady state temperatures and compositions for C/O = 0.6.

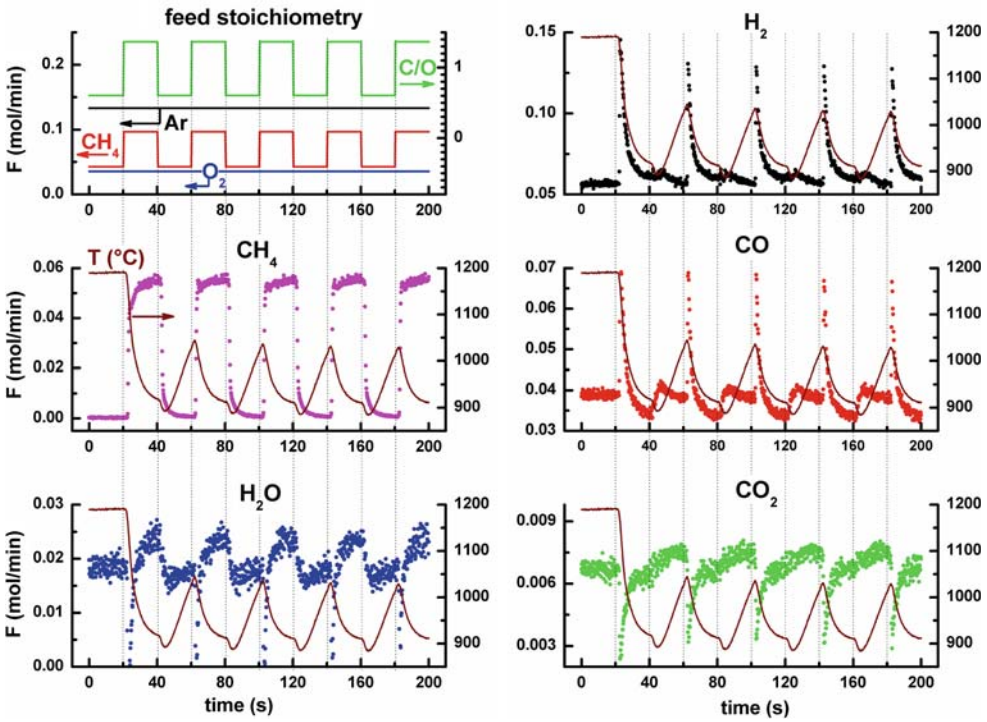

Figure 3. Transient integral experiment for methane on Rh. Profiles were measured for a stepwise switch of C/O 0.6 ↔1.4 with 20 s at each C/O. Temperature (T) and species profiles (H_2, CH_4, CO, H_2O, CO_2) at the end of the catalyst (x = 10 mm) are shown.

At steady-state, a temperature of ~1190 °C is measured at the end of the catalyst. After switching from steady state at C/O = 0.6–1.4, the temperature decreases exponentially towards the new steady state of the higher C/O ratio. At t = 40 s, the C/O ratio is switched back to 0.6. Surprisingly, before the temperature starts to rise according to the lower C/O it dips for 5 s by about 25 °C. Because 20 s is too short for the system to completely reach either steady state, the alternating switches between the two C/O ratios leads finally to a temperature oscillation around the steady state value of the mean C/O ratio of 1.0. All switches show the exponential temperature drop after switching to C/O = 1.4, the temperature dip following the switch back to 0.6 and a near linear rise in temperature at C/O = 0.6.

For all switches from 0.6 to 1.4 the partial oxidation products H_2 and CO show sharp overshoots, while the total oxidation products H_2O and CO_2 show sharp undershoots. The peaks reach their maxima or minima respectively within 0.5 s. No time phase shift between the peaks is observed. After peaking all products approach their new steady states exponentially, similar to the temperature results.

The responses to the switches from C/O = 1.4 to 0.6 have a much smaller amplitude and have more complicated structures. CO shows a small but noticeable overshoot that occurs when the temperature dips immediately after switching back from 1.4 to 0.6. Then CO declines towards the steady state of C/O = 0.6. H_2 shows a small overshoot as well. H_2O drops below the steady state value of C/O = 0.6 immediately after the switch and rises than back to it. CO_2 rises nearly linearly for about 15 s after switching back to C/O = 0.6 but then declines leading to a broad and indistinct maximum. The CO_2 signal is generally very low so that the maxima are nearly obscured by experimental noise.

O_2 variations are not observed at the end of the catalyst because O_2 conversion reaches completion in all situations. By switching from C/O = 0.6 to 1.4, CH_4 conversion becomes incomplete and a breakthrough occurs. The CH_4 rise consists of a very steep edge caused by the higher CH_4 flow rate stepped into the reactor and a slower rising part caused by decreasing methane conversion during the cooling period at C/O = 1.4. After switching back to 0.6, CH_4 drops quickly close to zero due to the lower flow rate and approaches zero because of the rising temperature (rising methane conversion).

3.3. Spatio-temporal profiles: methane on Rh

The transient experiment described above was also performed at 15 different positions along the axis of the heat shield/catalyst stack to obtain a complete spatio-temporal response surface for each species and temperature. As an example, figure 4 shows the response surfaces for temperature, CH_4, H_2, and O_2. For clarity, only three switches are shown.

The temperature plot shows that the temperature rises steeply at the catalyst entrance and declines slowly towards the exit of the back heat shield. At a steady state of C/O = 0.6, the maximum temperature of the gases (~1300 °C at x = 6 mm) is about 300 °C higher than when the gases leave the back heat shield (x = 20 mm). The temperature modulations are strongest in the middle of the catalyst and are damped towards the entrance and the exit. There is also an increasing phase shift between temperature and C/O ratio towards the end of the back heat shield (x = 20 mm). At the exit of the catalyst (x = 10 mm), C/O and temperature are still in phase, i.e. the temperature maximum occurs during the C/O = 0.6 period (see figure 3). At x = 20 mm the phase shift causes the temperature to peak during the C/O = 1.4 period and to reach a minimum during C/O = 0.6.

The response surfaces of the reactants reflect how the CH_4 flow was stepped in the feed, whereas O_2 was fed at constant flow rate (-5 mm $< x <$ 0 mm). For all steps, O_2 is fully converted within a few mm of the catalyst (x > 0 mm). CH_4 is fully converted for C/O = 0.6, while at C/O = 1.4 some CH_4 breakthrough occurs. The H_2 response surface (upper right corner) shows the sharp H_2 overshoots in time. In the axial direction, H_2 rises steeply within the first 5 mm of the catalyst and approaches then slowly its outlet value (see the axial profiles in figure 2 for comparison).

4. Discussion

4.1. Sampling technique

In this work axial species concentrations and temperatures are measured by sliding a fused silica capillary through a small channel drilled through the foam monoliths comprising the reactor bed (Figure 1). The fused silica capillary serves as a duct to continuously sample species into a mass spectrometer and as an access point for a thermocouple to measure temperature at the species sampling location. High spatial resolution is achieved by a precise axial positioning using a micrometer and a very small sampling orifice (d~0.3 mm).

In addition to measuring spatial profiles, the capillary sampling technique also provides the opportunity to follow rapid species and temperature changes in transient reactor operation. High temporal resolution is achieved because (1) the mixing volume of the capillary system is very small (< 0.2 ml), (2) the sampled gases are forced to flow directly over the sapphire seat of the high vacuum valve, and (3) the rapid data acquisition rate associated with the mass spectrometer and data analysis system.

With any analysis technique the hope is that the disturbance to the system is minimal so that measured values reflect the studied process and not artifacts of the

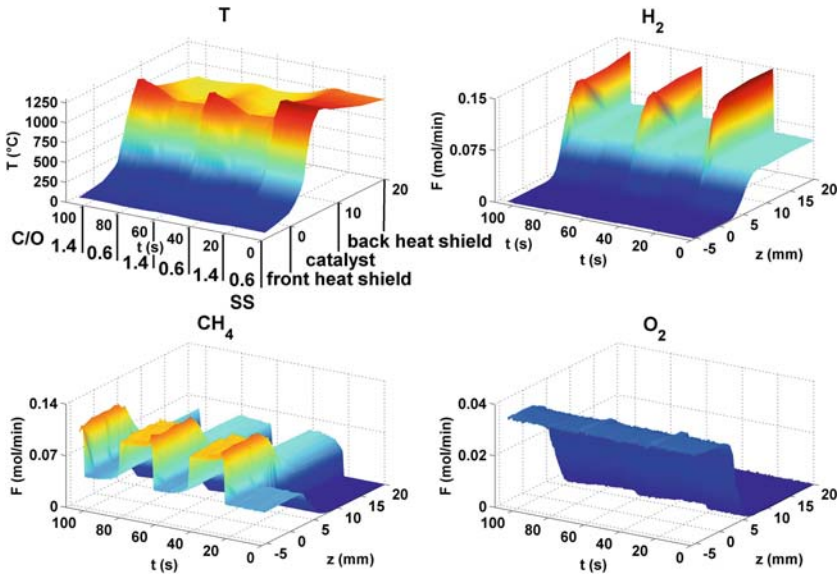

Figure 4. Spatio-temporal experiment for methane on Rh. Temperature (T) and species profiles (H_2, CH_4, CO, H_2O, CO_2) at 15 points within the catalyst/heat shield stack were measured for a stepwise switch of C/O 0.6↔1.4 with 20 s at each C/O. The smooth response surfaces were generated by interpolating between the data points using Matlab.

technique. Some details about the collected data are not completely understood yet since this is a new sampling technique. For example, many heat transfer phenomena are going on inside the reactor and are influencing the actual temperature of the thermocouple junction such as (1) conduction axially through the thermocouple and the quartz capillary, (2) radiation from the hot catalyst surface through the quartz capillary to the thermocouple, and (3) convective heat transfer. The temperature measured by the thermocouple is believed to be biased towards the gas temperature as opposed to the catalyst surface temperature. This is important to consider because the temperature of the gas near the entrance of the catalyst has probably not equilibrated to the temperature of the surface. Although it is not known exactly how the measured temperature corresponds to the actual system temperature, valuable information can be obtained from temperature data such as presence/location of temperature maxima inside the catalyst. The K type thermocouple is sheathed in inconel, an alloy containing ~70% nickel. Because nickel is known to be an effective reforming catalyst, the reactor and sampling system were designed such that there is a minimal amount of hot thermocouple in contact with sampled gas. Reactant gasses flow up around the quartz sampling capillary keeping all of the capillary cool except that portion which is inside the hot catalyst (Figure 1). Experiments performed in this way with and without a thermocouple (not shown) indicate that chemistry on the thermocouple minimally impacts the measured reaction products.

Another detail of the system, which is not completely understood, relates to the resolution of the sampling technique. Although the linear resolution of the movement device is on the order of 0.01 mm (or less), the size of the sampling hole in the side of the capillary and the spacing of pores in the monolith most likely dominate the ultimate resolution of this sampling technique. Minimum spatial resolutions of 0.12–0.3 mm are shown in the steady state experiments presented in figure 2. This capillary side sampling technique ensures that there is no void left behind the sampling location as would be the case if the capillary was left completely open at the sampling point.

The particular value of the spatial (2D) and spatio-temporal (3D) data presented in this study is their much higher information content in comparison to steady state integral reactor data (1D) commonly presented for such high temperature reactions. Correct prediction of spatial and spatio-temporal data by numerical simulation makes a much greater demand on the correctness of both the multi-step reaction model and the description of the transport processes. The immense number of degrees of freedom in a multi-step heterogeneous and homogeneous reaction model with dozens, hundreds or even thousands of reaction steps requires experimental data with high information content to validate the model.

Some of the profiles presented in this work show structure (e.g., methanation on Rh) that is not predicted by current models or our current understanding of the mechanisms of partial oxidation reactions. A comparison of the measured spatial profiles of methane on Rh and current surface models is made in another work [36]. The mechanistic interpretation of all structures observed in the spatial and spatio-temporal data will

require additional experiments to characterize the effects of various parameters (flow rates, C/O, catalyst, support, etc.). Also, development of more detailed models will be necessary to describe these data. Within the scope of the work presented here, the most remarkable features observed in the higher dimensional data are simply commented on.

4.2. Steady state spatial profiles: CH_4 on Rh vs. CH_4 on Pt

There is unexpected fine structure in the steady state spatial profiles. All results shown have been repeated on at least three catalysts in two independent experimental reactor systems. None of the structures appear to be an artifact of a particular catalyst or of the sampling technique. Possible voids in the catalyst or regions of low or high metal loading which could produce regions of low or high activity were an obvious concern. However, good overall reproducibility between catalysts was observed, indicating that these effects are negligible.

Rh is generally a superior catalyst for syngas than Pt. The spatial profiles in figure 2a and b show that CH_4 conversion and syngas selectivity is higher on Rh than on Pt, and O_2 and CH_4 are both consumed faster on Rh than on Pt. The most notable feature of CH_4 reaction on Rh is the presence of coincident peaks for CH_4 and H_2O (positive) and H_2 and CO (negative) between 4 and 7 mm in the catalyst. In this region, H_2 and CO are consumed to form CH_4 and H_2O (methanation: $3H_2 + CO \rightarrow CH_4 + H_2O$). The ratio of H_2/CO consumption in this zone reflects to a good approximation the 3/1 stoichiometry of this reaction. Little or no evidence of methanation is observed on the Pt catalyst without washcoat. Experimental data for Rh indicate that the presence of a washcoat enhances the methanation (data not shown).

It is believed that methanation is possible because of the lower surface temperatures of the rhodium catalyst compared to platinum. Comparisons of washcoated and non-washcoated (not shown) catalysts indicate that carbon deposits or metal dispersion may also play a role because methanation is more prominent on washcoated catalysts. Isothermal equilibrium calculations performed with the measured reactor compositions at 3.75 mm, show that methanation is favored at a temperature of 620–630 °C. Although this is lower than the measured temperature at this location of 695 °C the calculations show that methanation is thermodynamically feasible. Following the methanation zone there is a steam reforming zone producing H_2 and CO.

4.3. Ethane on Pt

Previous experiments [20,37,38] and models [10,12,39] suggest that ethylene is formed primarily by homogeneous reactions, and that the initial reactions are primarily partial or total oxidation to produce H_2, H_2O, CO, and CO_2 that generates the heat required for dehydrogenation. Ethane oxidation at higher C/O ratios also exhibits some O_2 breakthrough, and figure 2c shows that O_2 is consumed much more slowly with ethane than with methane.

There is essentially no formation of ethylene in the first 3 mm of the catalyst, and approximately 75% of the O_2 is consumed before any ethylene is formed. The point of beginning ethylene formation at $x \sim 3$ mm is further characterized by a drop in the oxygen conversion rate and a leveling off of the temperature. Throughout the catalyst and back heat shield the measured temperature continues to rise monotonically indicating that the global chemistry of the system is essentially exothermic along the entire length of the catalyst. The product distribution, with little water production after 3 mm, suggests that ethylene is produced by dehydrogenation ($C_2H_6 \rightarrow C_2H_4 + H_2$) instead of oxidative dehydrogenation ($C_2H_6 + 1/2O_2 \rightarrow C_2H_4 + H_2O$). Furthermore, consumption of ethane and formation of species in the back heat shield (> 10 mm) where there is no catalytic metal and after oxygen has all been consumed indicates the importance of dehydrogenation reactions in the formation of ethylene. Methane formation in the back heat shield also suggests that CH_4 is formed homogeneously from ethane.

4.4. Transient and spatio-temporal profiles

In previous publications transients in the startup of short contact time reactors for methane [32] and higher hydrocarbons [33] have been followed monitoring the catalyst exit composition with mass spectrometry. The experiments presented here are different as catalyst and reaction, initially at steady state at a particular C/O ratio, are suddenly disturbed by switching to a different C/O ratio with a different steady state temperature and composition.

In figures 3 and 4 the C/O ratio was changed periodically from 0.6 to 1.4, and the responses in temperature and composition were measured. The changes in stoichiometry were realized within 0.5 s, which sets the lower limit for the time resolution of this experiment. As can be expected from the high rate by which the methane CPO proceeds (ms timescale), the responses of the different species to the stoichiometry switches do not directly reflect the kinetics of any particular reaction in the complex reaction network. The observed sharp overshoots and undershoots for H_2/CO and H_2O/CO_2, respectively, upon each switch from C/O = 0.6 to 1.4 are indeed exactly in phase indicating that the chemistry follows the new stoichiometry nearly instantaneously. The transients resolve how the chemistry follows catalyst heating and cooling and how carbon deposits influence the activity of the catalyst and its temperature profile.

4.4.1. Temperature transients

The assignment of the temperatures measured with the capillary technique to the gas or surface is not unique. The thermocouple is not in direct thermal contact with the surface; although, it sees radiation from the surface. Numerical simulations indicate that the thermocouple measurements are skewed towards the gas phase rather than the surface temperature [18].

The temperature profiles (Figure 2 and 4 upper left panel) illustrate how steep the temperature gradients in the catalyst are. Within a few mm, the temperature rises from room temperature to more than 1300 °C. Heat is generated in the front section of the catalyst where oxidation reactions occur (see O_2 surface lower right panel).

If the C/O ratio is stepped temperature oscillations occur. The upper left panel in figure 4 shows that the amplitude of the oscillations is highest in the middle of the catalyst ($x \sim 5$ mm) and is damped towards the front and back heat shield. In addition to the damping a phase shift occurs towards the back heat shield. The heat travels like a wave downstream leading to an increasing phase shift with increasing axial coordinate. The temperature damping with increasing distance from the oxidation zone can be explained by the finite rate of heat conduction in the solid material. The phase shift can only be explained if the distance between the heat generating zone and the thermocouple changes by stepping the C/O ratio.

The phase shift is seen in the transient measurement at the end of the catalyst ($x = 10$ mm, figure 3) even better than in the three dimensional plot. After switching from C/O = 1.4 back to 0.6 the temperature trace shows a dip that is in contrast to the expectation. The catalyst operates much hotter at C/O = 0.6 than at 1.4 and the temperature should increase instantaneously. An explanation for the dip is a change in location of the oxidation zone in the catalyst. A possible reason for that can be given by looking at the species transients.

4.4.2. Species transients

The species transients shown in figure 3 will be discussed separately for switches from C/O = 0.6 to 1.4 and from C/O = 1.4 to 0.6. The sharp overshoots for H_2 and CO by feeding suddenly a methane rich mixture to the hot catalyst (step from C/O = 0.6 to 1.4) can be understood by taking into account that high temperatures favor the formation of partial oxidation products H_2, CO over the total oxidation products H_2O and CO_2. As the catalyst cools rapidly, the peaks are very narrow (~5 s). The decline of the flow rates of H_2 and CO after the switch 0.6 $\rightarrow$ 1.4 is nearly a mirror image of the incline of the flow rates of CH_4 and H_2O. This synchronized behavior indicates that steam reforming ($CH_4 + H_2O \rightarrow 3H_2 + CO$, $\Delta H_r^\circ = +206$ kJ/mol) is a source of H_2 and CO formation as was also concluded from the spatial profiles. The traces of H_2, CO, H_2O, and CH_4 reflect how the steam reforming equilibrium follows the decreasing catalyst temperature. All peaks being in phase temporally indicates that even a 50–100 ms time resolution is too slow to follow the kinetics of particular reaction steps. The sharp undershoot of CO_2 at every step from 0.6 to 1.4 is understandable because at C/O = 1.4, more C atoms at the surface compete for the O atoms making it more unlikely for one C atom to bind two O atoms.

The reverse switch from 1.4 to 0.6 shows a distinct overshoot in CO but only a small overshoot in H_2. CO_2 shows a small overshoot as well. The peaking of the carbon oxides may indicate the burnoff of carbon deposited formed during the foregoing switch from C/O = 0.6 to 1.4. At C/O = 0.6 the catalyst surface temperature is higher than 1300 °C. If a feed with a C/O = 1.4 is now suddenly passed over the hot catalyst, not all C atoms can combine with O atoms to form CO or CO_2. They rather form a multilayer of carbon on the catalyst surface. The switch back to C/O = 0.6 restores the catalytically active sites that were blocked by carbon. For a short moment, O_2 can not oxidize H_2 to H_2O because it is consumed by the carbon burnoff leading to a small but noticeable H_2 overshoot before H_2 production goes down due to increasing H_2O formation. The CO overshoots are stronger because of the carbon burnoff. The reversible deactivation of the catalyst entrance by carbon deposits is also in agreement with the phase shifts observed in the temperature transients because it appears that the oxidation zone moves suddenly away from the thermocouple towards the catalyst entrance.

4.5. Surface coverages

Much of the unexpected fine structure in these results may be due to rapid changes in surface coverages with position. As examples, O, CO, and C are predicted to be the dominant species at different regions within the catalyst [9,36] for methane on Rh, and these coverages are strong functions of the surface temperature and C/O/H ratios.

In particular, carbon formation within the catalyst after all or most of the O_2 has reacted appears to inhibit surface reactions and allow more gas phase reactions to occur. This carbon could be sub-monolayer, but preliminary thermal and chemical titration experiments (data not shown) indicate that multilayer carbon forms near the back of the catalyst, particularly at high C/O and in regions of lower catalyst temperatures. While detailed models predict these coverages (but not multilayer C), transitions in coverage with position may be sharper than models predict. The effects of feed stoichiometry (C/O ratio), catalyst loading, and time on stream on carbon coverages are currently being evaluated and will be presented systematically in a future work.

5. Conclusions

Spatial and spatio-temporal data have much more information content than integral steady state data measured at the reactor outlet. This work demonstrates how these data can be measured by combining a rapid scanning mass spectrometer with a capillary sampling technique. Temperature and species profiles can be measured with high spatial resolution (< 0.3 mm), while transients can be followed with a time resolution down to 50 ms. Catalyst phenomena that can only be revealed by high-resolution spatial or spatio-temporal measurements have been highlighted and mechanistic interpretations have been made.

The capability to measure species and temporal profiles is critical in interpreting the mechanism for millisecond reactors and in designing new processes. This is especially true because profiles vary so rapidly compared to conventional packed bed reactors. Chemical parameters such as metal loading, support material, additives, and impurities have an important role. Geometric parameters such as pore size, flow rate, preheat, and catalyst stratification have been shown to have large effects on performance that may be interpreted through spatial profiles. The role of carbon in affecting performance (such as increasing or decreasing the amount of homogeneous reaction and olefin formation) has a dominant role with higher hydrocarbon fuels. Renewable fuels have very different functionalities and reaction channels compared to hydrocarbons that need to be characterized. Combining the capillary sampling with GC analysis is currently under investigation to measure spatial resolved data for species requiring separation before analysis (e.g. liquid fuels, renewable fuels). Finally, the design and optimization of industrial reactors can be carried out by finding how these parameters affect performance and catalyst durability. Transient operation has an obvious role in both process diagnostics and in developing industrial processes that may operate in transient modes.

Acknowledgments

Funding for this work was provided in part by the United States Department of Energy (DOE Grant # DE-FG02-88ER13878).

References

[1] L.D. Schmidt, J. Siddall and M. Bearden, AIChE J. 46 (2000) 1492.
[2] D.J. Wilhelm, D.R. Simbeck, A.D. Karp and R.L. Dickenson, Fuel Process. Technol. 71 (2001) 139.
[3] T.H. Fleisch, R.A. Sills and M.D. Briscoe, J. Nat. Gas Chem. 11 (2002) 1.
[4] J.P. Lange, R.J. Schoonebeek, P.D.L. Mercera and F.W. van Breukelen, Appl. Catal. A–Gen 283 (2005) 243.
[5] D.A. Hickman and L.D. Schmidt, AIChE J. 39 (1993) 1164.
[6] O. Deutschmann and L.D. Schmidt, AIChE J. 44 (1998) 2465.
[7] C.T. Goralski, R.P. O'Connor and L.D. Schmidt, Chem. Eng. Sci. 55 (2000) 1357.
[8] O. Deutschmann, R. Schwiedernoch, L.I. Maier and D. Chatterjee, Stud. Surf. Sci. Catal. 136 (2001) 251.
[9] R. Schwiedernoch, S. Tischer, C. Correa and O. Deutschmann, Chem. Eng. Sci. 58 (2003) 633.
[10] M.C. Huff, I.P. Androulakis, J.H. Sinfelt and S.C. Reyes, J. Catal. 191 (2000) 46.
[11] D.K. Zerkle, M.D. Allendorf, M. Wolf and O. Deutschmann, J. Catal. 196 (2000) 18.
[12] F. Donsì, K.A. Williams and L.D. Schmidt, Ind. Eng. Res. Chem. 44 (2005) 3453.
[13] F. Basile, G. Fornasari, F. Trifiro and A. Vaccari, Catal. Today 64 (2001) 21.
[14] L. Basini, K. Aasberg-Petersen, A. Guarinoni and M. Ostberg, Catal. Today 64 (2001) 9.
[15] M. Bizzi, L. Basini, G. Saracco and V. Specchia, Chem. Eng. J. (Amsterdam, Netherlands) 90 (2002) 97.
[16] S. Marengo, P. Comotti and G. Galli, Catal. Today 81 (2003) 205.
[17] B. Li, K. Maruyama, M. Nurunnabi, K. Kunimori and K. Tomishige, Appl. Catal. A–Gen. 275 (2004) 157.
[18] M. Bizzi, G. Saracco, R. Schwiedernoch and O. Deutschmann, AIChE J. 50 (2004) 1289.
[19] E.J. Klein, S. Tummala and L.D. Schmidt, Stud. Surf. Sci. Catal. 136 (2001) 245.
[20] D.A. Henning and L.D. Schmidt, Chem. Eng. Sci. 57 (2002) 2615.
[21] T.C. Bond, R.A. Noguchi, C.-P. Chou, R.K. Mongia, J.-Y. Chen, and R.W. Dibble, Symposium (International) on Combustion, [Proceedings], 26th (1996) 1771.
[22] M. Lyubovsky, S. Roychoudhury and R. LaPierre, Catal. Lett. 99 (2005) 113.
[23] A.B. Mhadeshwar and D.G. Vlachos, J. Phys. Chem. B 109 (2005) 16819.
[24] R.W. Sidwell, H. Zhu, B.A. Kibler, R.J. Kee and D.T. Wickham, Appl. Catal. A–Gen. 255 (2003) 279.
[25] R.W. Sidwell, H. Zhu, R.J. Kee and D.T. Wickham, Combust. Flame 134 (2003) 55.
[26] M. Reinke, J. Mantzaras, R. Schaeren, R. Bombach, A. Inauen and S. Schenker, Combust. Flame 136 (2004) 217.
[27] M. Reinke, J. Mantzaras, R. Bombach, S. Schenker and A. Inauen, Combust. Flame 141 (2005) 448.
[28] J.D. Grunwaldt and A. Baiker, Catal. Lett. 99 (2005) 5.
[29] J.D. Grunwaldt, S. Hannemann, C.G. Schroer and A. Baiker, J. Phys. Chem. B 110 (2006) 8674.
[30] A.S. Bodke, S.S. Bharadwaj and L.D. Schmidt, J. Catal. 179 (1998) 138.
[31] A.E. Schweizer and G.T. Kerr, Inorg. Chem. 17 (1978) 2326.
[32] K.A. Williams, C.A. Leclerc and L.D. Schmidt, AIChE J. 51 (2005) 247.
[33] K.A. Williams and L.D. Schmidt, Appl. Catal. A–Gen. 299 (2006) 30.
[34] V.H. Dibeler, *Mass Spectrometry*, ed. C.A. McDowell. 1963, New York: McGraw-Hill.
[35] J.M. Ruth, Anal. Chem. 40 (1968) 747.
[36] R. Horn, K.A. Williams, N.J. Degenstein and L.D. Schmidt, J. Catal. in press (2006).
[37] A. Beretta, E. Ranzi and P. Forzatti, Chem. Eng. Sci. 56 (2001) 779.
[38] A. Beretta, E. Ranzi and P. Forzatti, Catal. Today 64 (2001) 103.
[39] C.A. Mims, R. Mauti, A.M. Dean and K.D. Rose, J. Phys. Chem. 98 (1994) 13357.